

Structural Characteristics of Coal Vitrinite during Pyrolysis

Wu Li*,†,‡,§ and Yanming Zhu†,‡

†School of Resources and Earth Science, China University of Mining & Technology, Xuzhou 221008, People's Republic of China

‡Key Laboratory of Coalbed Methane Resource & Reservoir Formation Process, Ministry of Education, Xuzhou 221116, People's Republic of China

§School of Chemical Engineering, the University of Queensland, Brisbane, Queensland 4072, Australia

ABSTRACT: Vitrinite samples inserted into a furnace at room temperature and heated at a rate of 10 °C/h were subjected to X-ray diffraction analysis, Fourier transform infrared spectroscopy (FTIR), and solid-state ^{13}C nuclear magnetic resonance spectroscopy (^{13}C NMR) to characterize the macromolecular structure of vitrinite of different ranks of coal, which was discussed with respect to changes in its chemical structure. The results demonstrate that the relationship between average reflectance of the vitrinite and temperature is linear. The structural parameters of vitrinite separated from the coking coal sample collected from the Luijiaotuo mine (LJTV) ($d_{002} = 3.56 \text{ \AA}$, $L_c = 11.62 \text{ \AA}$, $L_a = 10.99 \text{ \AA}$) were obtained. The FTIR spectra include bands characteristic of aliphatic C–H stretching, with the ratio of aliphatic oxygen-containing compounds decreasing with increasing rank of the vitrinite samples. The C=O stretching contribution is lower than the aliphatic C–H stretching contribution, whereas the aromatic carbon contribution is high in all of the samples. The vitrinite structural parameters, e.g., the A factor, C factor, CH_2/CH_3 , $A_{\text{ar}}/A_{\text{al}}$, Al/OX, Al/C=C, and C=O/C=C, were calculated. The intensity of the aromatic carbon peak is considerably greater than that of the aliphatic carbon peak. The ^{13}C NMR spectra reveal that the aliphatic carbon content decreases progressively with increasing thermal maturity for the replacement of aromatic hydrogens by condensation. The CCH_3 groups are removed more slowly than are the $\text{C}(\text{CH}_2)\text{C}$ groups. The coalification progress was divided into two stages based on the CH_2/CH_3 ratio, which first decreases and later increases. As revealed by the structural parameter f_a , the aromaticity of vitrinite increases during pyrolysis.

1. INTRODUCTION

Changes in the organic geochemistry, geology, and physical and chemical structure of coals during coalification have been extensively investigated in many countries throughout the world.^{1–3} In previous studies on the organic geochemistry of coal, XRD, FTIR, and ^{13}C NMR have been commonly used to characterize the functional groups and structural parameters in kerogen and macerals.^{4,5} ^{13}C NMR spectroscopy has been used for coal research since the late 1970s.^{6–8} Cao et al. studied the response of chemical structure changes in kerogen from bituminous coal on dike intrusions and reviewed the characterization of kerogen using advanced ^{13}C NMR spectroscopy.^{9,10} FTIR spectroscopy was used to understand the effect of sample structure on absorptivity for aromatic and aliphatic C–H bonds¹¹ and coal aromaticity and to analyze the carboxyl groups.¹² The chemical structure of perhydrous coals was investigated by FTIR and Py-GC/MS. Reactive functional groups and aliphatic hydrocarbons were released with increasing pyrolysis temperature.¹³ In a later study, the structural characteristics of thermally metamorphosed coal were investigated using FTIR spectroscopy and XRD analysis.¹⁴ Recently, the structures of chars in inertinite-rich coal were characterized by X-ray diffraction.¹⁵

The structural characteristics of the vitrinite and inertinite before and after pyrolysis were studied by ultimate analysis, FTIR, and ^{13}C NMR.¹⁶ An FTIR spectrometer equipped with a microscope in reflectance mode was used to analyze the chemical structure of individual coal macerals, including liptinite, vitrinite, semifusinite, and inertinite.¹⁷ The evolution of the coal structure during the coalification process can be assessed using FTIR spectroscopy.¹⁸ Walker et al.¹⁹ found that, when Pennsylvanian

coal samples were heated to 425 °C, liptinites in vitrinites disappear and concomitantly change into vesicles. Certain functional groups (e.g., broad hydroxyl and aliphatic stretching regions) disappear as the temperature increases. The evolution of the optical properties of vitrinite in response to heating was systematically characterized by Komorek et al.^{20,21} Rachel et al.²² analyzed individual maceral chemistry and functional groups of high volatile southern Indiana bituminous coals. Morga et al.²³ reported the chemical structure evolution of fusinite and semi-fusinite with higher aromaticity at high temperatures. However, only a few studies have addressed the chemical structure evolution in the coalification of single vitrinite and the mathematical characteristics of chemical structure parameters.

The present work concentrates mainly on the analysis of vitrinite, a single maceral in coal. The structural evolution of vitrinite of different ranks during pyrolysis was obtained, which is useful for achieving a profound understanding of the coalification process. More importantly, the chemical data lend themselves to statistical analyses with the potential to answer questions about high-coal-rank vitrinite formation. The objectives of the present work were (1) to investigate the changes in the chemical structure of vitrinite isolated from coking coal that occurred during heat treatment from room temperature to 550 °C using XRD, FTIR, and ^{13}C NMR; (2) to quantitatively analyze the functional groups, carbon types, and structural evolution of the product, which are valuable for the

Received: February 1, 2014

Revised: May 21, 2014

Published: May 21, 2014



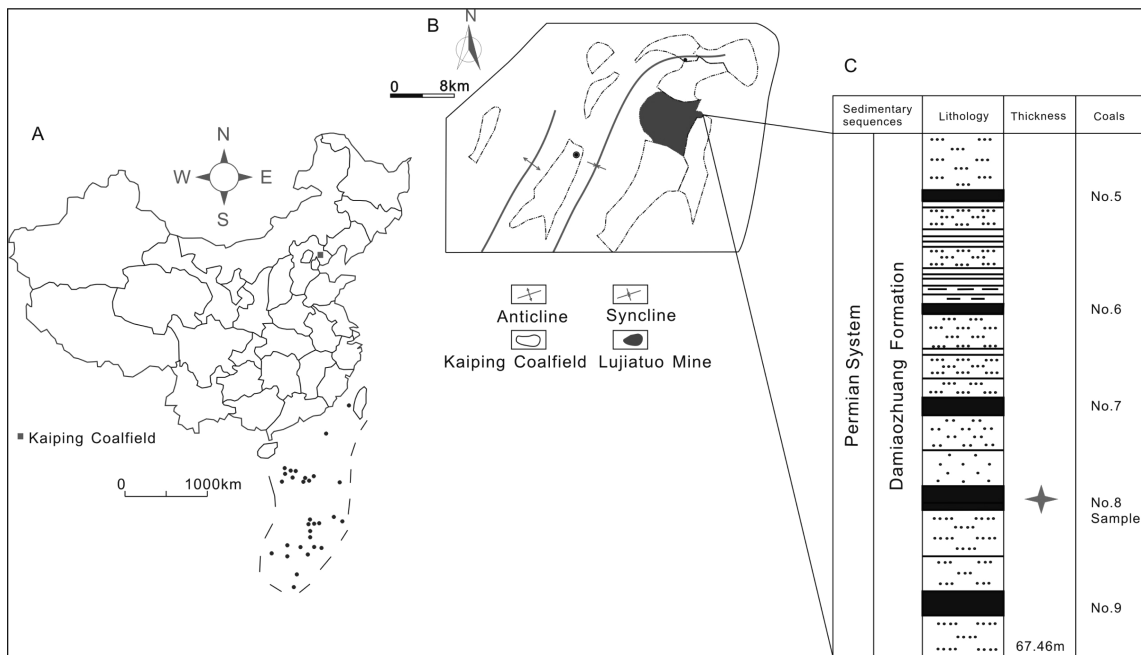


Figure 1. Location of Kaiping Coalfield in the North China plate (A). Location of the Lujiatuo Mine in the Kaiping Coalfield (B). Sedimentary sequences in the Lujiatuo Mine (C).

Table 1. Results of Rock-Eval Pyrolysis and Proximate and Ultimate Analyses for Sample LJTV^a

coal sample	Ro,max	proximate analysis					ultimate analysis			
		M _{ad}	A _d	V _{daf}	Q _{gr,d}	C _{daf}	H _{daf}	O _{daf}	N _{daf}	
LJTV	1.61	0.66	18.37	27.35	25.30	87.24	5.29	5.17	1.63	

^aRo,max: maximum reflectance of vitrinite (%); M_{ad}: moisture content (wt %, air-dried basis); A_d: ash content (wt %, dry basis); V_{daf}: volatile content (wt %, dry ash-free basis); Q_{gr,d}: gross calorific value (MJ/kg, dry basis); C_{daf}: carbon content (wt %, dry ash-free basis); H_{daf}: hydrogen content (wt %, dry ash-free basis); O_{daf}: oxygen content (wt %, dry ash-free basis); N_{daf}: nitrogen content (wt %, dry ash-free basis).

modeling of coalification processes; and (3) to investigate the changes in the structural parameters (e.g., CH₂/CH₃ and f_a) with increasing coal rank.

2. GEOLOGICAL SETTING

The Permo-Carboniferous Kaiping Coalfield, which is 35 km long and 28 km wide, with a total area of 812 km² (Figure 1A), is located in the North China plate (Figure 1A). The Lujiatuo Mine, which belongs to Kailuan Group Co., is located in the eastern part of this coalfield and covers an area of 39.7 km². The main minable coal beds are Nos. 7, 8, 9, and 12.

The coal-bearing Permian sequences are collectively called the Shanxi Group and generally include the Damiao Zhuang formation. Five coal beds are found in the Damiao Zhuang formation: Nos. 5, 6, 7, 8, and 9.

3. SAMPLES AND EXPERIMENTS

3.1. Sample and Preparation. One bench sample of coking coal was obtained from the face of the No. 8 coal bed at Lujiatuo Mine in Kaiping Coalfield (LJT) following the Chinese Standard Method GB/T482-2008. The sampling position is located in the No. 5885 coal face at ~800 m, where there is no geological structure (e.g., faults, magmatite). The size of the coal bench sample is 20 cm × 20 cm × 10 cm. All collected samples were immediately placed in a polyethylene bag filled with nitrogen gas to minimize oxidation and contamination. The separation of the vitrinite sample (LJTV) from LJT is based on the method reported by Li et al.²⁴ High-purity vitrinite was obtained by the density gradient centrifugation (DGC) method. The high and low densities of zinc chloride are 1.36 and 1.30 g/cm³, respectively.

Proximate and ultimate analyses of LJTV were conducted based on the standards put forward in 2006 and 2008 (GB/T212-2008, CB/T476-2008, GB/T213-2008, GB/T19227-2006). Vitrinite reflectance was tested following the Chinese Standard Method GB6948-2008. The results for sample LJTV are presented in Table 1.

3.2. X-ray Diffraction Analysis. The XRD data collection of LJTV was performed by a D8 ADVANCE (Bruker) instrument with a Cu target and K α radiation at the Advanced Analysis and Computation Center at the Chinese University of Mining and Technology. The operating conditions of the X-ray tube are U = 40 kV and I = 30 mA. The size of the powdered sample is 300 mesh.

The crystallite structural parameters, interlayer spacing (d_{002}), average lateral sizes (L_a) and stacking heights (L_c), have been established, and the computing method is according to Li et al.²⁵

$$d_{002} (\text{\AA}) = \lambda / 2 \sin \theta_{002}$$

$$L_c (\text{\AA}) = 0.9\lambda / (\beta_{002} \cos \theta_{002})$$

$$L_a (\text{\AA}) = 1.84\lambda / (\beta_{100} \cos \theta_{100})$$

3.3. FTIR Analysis. The powdered sample (LJTV) was heated from room temperature to 550 °C at a heating rate of 10 °C/h. Twenty-two solid samples including one vitrinite sample (LJTV) and 21 residue vitrinite samples collected by the pyrolysis were subjected to FTIR spectra. The 21 residue vitrinite samples were named as LJTV-350, LJTV-360,...LJTV-550 every 10 °C from 350 to 550 °C.

Powdered coal (0.9 mg, under 200 mesh) was initially ground with 80 mg of potassium bromide (KBr) for 20 min in an agate mortar. The mixture was molded into a disc, and this powder was pressed into a transparent sheet for 10 min using a tablet machine. Pure ground KBr was used to obtain a reference spectrum. The discs were analyzed by

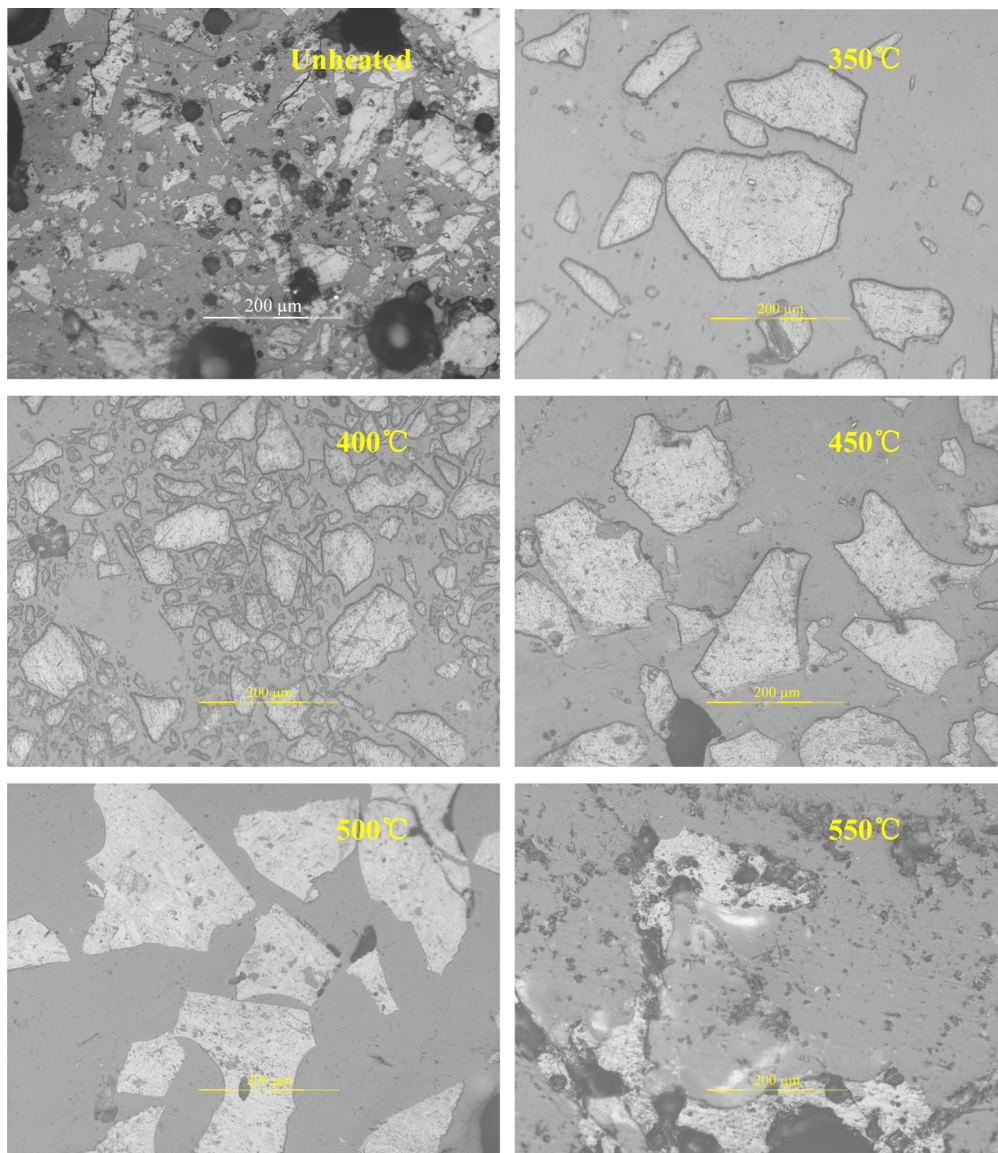


Figure 2. Solid vitrinite obtained at different heating temperatures (dry lens, objective 20×, eyepiece 10×).

FTIR (model VERTEX-70, made by Bruker in Germany), and the spectra were recorded in the range of 400–4000 cm⁻¹ at a resolution of 4 cm⁻¹.

The FTIR structural parameters, namely, the *A* factor, *C* factor, CH₂/CH₃, A_{ar}/A_{al}, Al/OX, Al/C=C, C=O/C=C, C=O cont, and C=C cont, were calculated from the peak area according to Suryendu et al.,²⁶ Xin et al.,²⁷ and Wang et al.²⁸

$$\begin{aligned} \text{A factor} = & (A_{3000-2800} \text{ cm}^{-1}) / (A_{3000-2800} \text{ cm}^{-1} \\ & + A_{1650-1520} \text{ cm}^{-1}) \end{aligned}$$

$$\begin{aligned} \text{C factor} = & (A_{1800-1650} \text{ cm}^{-1}) / (A_{1800-1650} \text{ cm}^{-1} \\ & + A_{1650-1520} \text{ cm}^{-1}) \end{aligned}$$

$$\text{CH}_2/\text{CH}_3 = (A_{2920} \text{ cm}^{-1}) / (A_{2950} \text{ cm}^{-1})$$

$$A_{\text{ar}}/A_{\text{al}} = (A_{1650-1520} \text{ cm}^{-1}) / (A_{2800-3000} \text{ cm}^{-1})$$

$$\text{Al}/\text{OX} = (A_{3000-2800} \text{ cm}^{-1}) / (A_{1800-1520} \text{ cm}^{-1})$$

$$\text{Al/C=C} = (A_{3000-2800} \text{ cm}^{-1}) / (A_{1650-1520} \text{ cm}^{-1})$$

$$\text{C=O/C=C} = (A_{1800-1650} \text{ cm}^{-1}) / (A_{1650-1520} \text{ cm}^{-1})$$

$$\text{C=O cont} = (A_{1800-1650} \text{ cm}^{-1}) / (A_{1800-1520} \text{ cm}^{-1})$$

$$\text{C=C cont} = (A_{1650-1520} \text{ cm}^{-1}) / (A_{1800-1520} \text{ cm}^{-1})$$

3.4. Solid-State Cross-Polarization Magic-Angle Spinning (CP/MAS) ¹³C NMR Analysis. ¹³C NMR of 22 solid vitrinite samples (LJTV, LJTV-350, LJTV-360, LJTV-370, LJTV-380, LJTV-390, LJTV-400, LJTV-410, LJTV-420, LJTV-440, LJTV-450, LJTV-460, LJTV-470, LJTV-480, LJTV-490, LJTV-500, LJTV-540) was measured. The ¹³C NMR spectra of vitrinite were obtained on a Bruker Avance III 400 spectrometer. All experiments were run in double-resonance probe heads using 4 mm sample rotors. Semiquantitative compositional information was obtained with good sensitivity by a ¹³C CP/MAS NMR in conjunction with the total sideband suppression (TOSS) technique (MAS = 4 kHz, contact time = 1 ms, recycle delay = 1 s). The ¹³C NMR structural parameters, *f*_d and A_{ar}/A_{al} were calculated from the peak area according to Cao et al.⁹ and Wang et al.²⁸

4. RESULTS AND DISCUSSION

4.1. Optical Characteristics of Vitrinite. Some electron microscopy images of the vitrinite pyrolysis products at different temperatures are shown in Figure 2. In the unheated vitrinite sample, the vitrinite particles exhibit smooth surfaces,

homogeneous optical properties, and the absence of pores. At 350 °C, the vitrinite particles still exhibit smooth polished surfaces with few pores but experience an obvious increase in reflectance. When the temperature is increased to 400 °C, some pores are observed in the vitrinite particles, and the polished surfaces became less smooth. The presence of vitrinite pores rapidly rises above 450 °C. Some vitrinite properties transfer into the new maceral properties.

The vitrinite reflectance increases in the pyrolysis process, similar to the results found for bitumen.²⁹ The vitrinite samples at temperatures up to 550 °C were characterized by the optical properties of the vitrinite with the same light intensity and a standard aperture diaphragm size to quantify the change in the vitrinite reflectance. We can see from Figure 3 that the

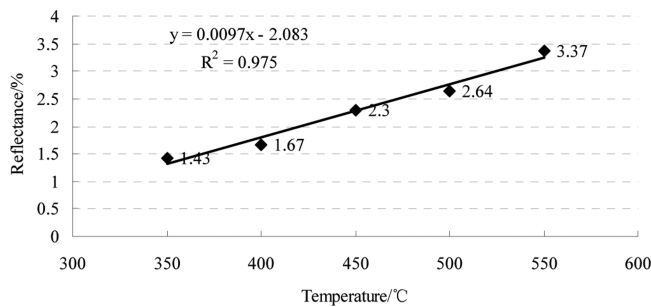


Figure 3. Relationship between pyrolytic temperature and vitrinite reflectance.

relationship between average reflectance and vitrinite pyrolytic temperature is linear ($R^2 = 0.975$). Consequently, the average vitrinite reflectance and pyrolytic temperature can be used to represent the thermal maturity.

4.2. Spectral Characteristics of Vitrinite of Different Maturities. Carbon Crystallite Properties. Figure 4 illustrates the representative XRD profiles of LJTV coal under heating. In

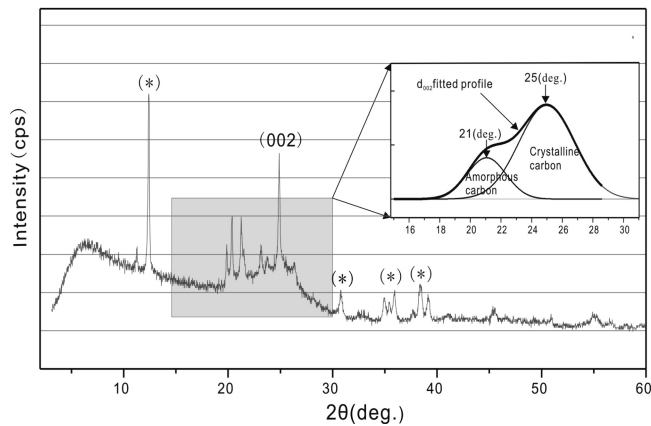


Figure 4. XRD profiles and deconvolution results for the 002 band of LJTV.

agreement with the results reported by other authors,^{30,31} the XRD profile has one obvious peak in the 2θ range of 15–30°, corresponding to the 002 plane. The 100 peak is in the 2θ range of 40–50°. There are also some narrow peaks centered at $2\theta = 12, 31, 35$, and 38° , corresponding to the 111, 220, 311, and 222 planes, respectively. The PFM module in Origin 7.5 software was used to deconvolute the diffractograms in the 2θ range of 15–30° to resolve 002. The deconvolution results for

LJTV coal is shown in Figure 4. The obtained structural parameters of carbon crystallite properties of LJTV are $2\theta_{002} = 25^\circ$, an interlayer spacing of 3.56 Å (d_{002}), a crystallite height of 11.62 Å (L_c), and a crystallite diameter of 10.99 Å (L_a).

Functional Groups Evolution during Pyrolysis. All vitrinite samples under heating feature a similar distribution of functional groups (Figure 5). Some spectra show a weak absorption at

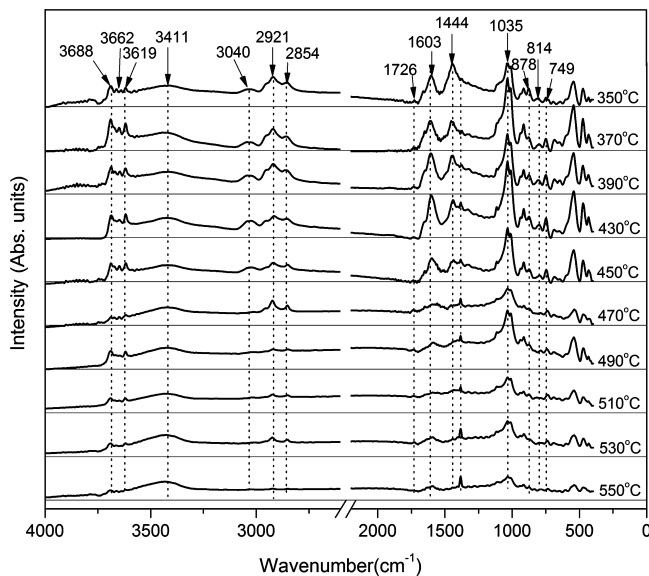


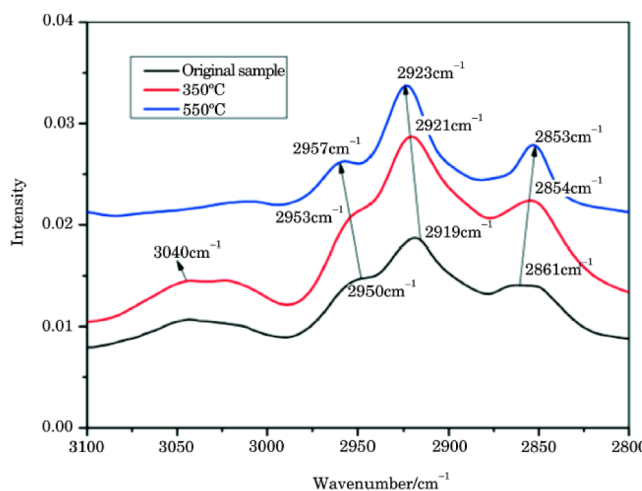
Figure 5. FTIR spectra of the vitrinite sample at different temperatures.

2360 cm⁻¹ due to the CO₂ in ambient air. The FTIR spectra of vitrinite LJTV-350 are characterized by strong aliphatic C–H stretching at 2921 and 2854 cm⁻¹, high-intensity aromatic (C=C) stretching vibrations at 1603 cm⁻¹, C–H aromatic out-of-plane deformation at 878 cm⁻¹ (assigned to the vibration of substituted aromatic rings with one adjacent C–H group), 814 cm⁻¹ (assigned to the vibration of substituted aromatic rings with two or three adjacent C–H groups), 749 cm⁻¹ (assigned to the vibration of substituted aromatic rings with four adjacent C–H groups), carbonyl/carboxyl C=O stretching at 1726 cm⁻¹, –OH stretching at 3411 cm⁻¹, and aromatic C–H stretching at 3040 cm⁻¹. The intense absorption peaks between 3000–2800 cm⁻¹ and 1520–1350 cm⁻¹ indicate an abundant contribution of alkyl chains. Three shoulder peaks (2953 cm⁻¹, aliphatic C–H stretching of –CH₃; 1091 cm⁻¹, C–O stretching; 730 cm⁻¹, polymethylenic chains ($n \geq 4$), rocking) can be observed (Table 2).

Figure 5 shows that, during pyrolysis, these vitrinites contain aliphatic structures in the region of 3000–2800 cm⁻¹, indicating strong aliphatic C–H stretching. The absorptions centered at 2854 and 2921 cm⁻¹ assigned to symmetric stretching vibrations and asymmetric stretching vibrations of –CH₂– methylene groups, respectively, are more intense in the coking coal vitrinite than in the vitrinite after pyrolysis. The peak due to aromatic C=C ring stretching is of moderate intensity and occurs at approximately 1603 cm⁻¹. The carbonyl and carboxyl C=O groups are represented by a weak absorption peak at approximately 1726 cm⁻¹ during pyrolysis. The absorptions of the asymmetric bending of –CH₃ and symmetric bending of –CH₂– centered at 1444 cm⁻¹ decrease with temperature. In contrast, the –CH₃ symmetric bending at approximately 1375 cm⁻¹, which is assigned to the symmetric deformational vibration of –CH₃ with a possible contribution from C–H

Table 2. Peak Assignments for the FTIR Spectra of LJTV-350

peak (cm^{-1})	band (cm^{-1})	assignments
3688, 3662, 3619	3700–3600	free –OH
3411	3500–3300	–OH stretching
3040	3055–3030	aromatic C–H stretching
2953 (shoulder), 2921, 2854	3000–2800	aliphatic C–H stretching
1726	1800–1650	carbonyl/carboxyl C=O stretching
1603	1650–1520	aromatic C=C ring stretching
1444, 1375	1520–1350	aliphatic –CH ₂ and –CH ₃ deformation
1329	1350–1250	aromatic ether C–O–C, phenolic C–O, and ester C–O–O–C stretching
1035, 1091 (shoulder)	1150–950	aliphatic ether C–O–C and alcohol C–O stretching
878, 814, 749	900–750	C–H aromatic out-of-plane deformation
730 (shoulder)	750–720	polymethylenic chains ($n \geq 4$) rocking

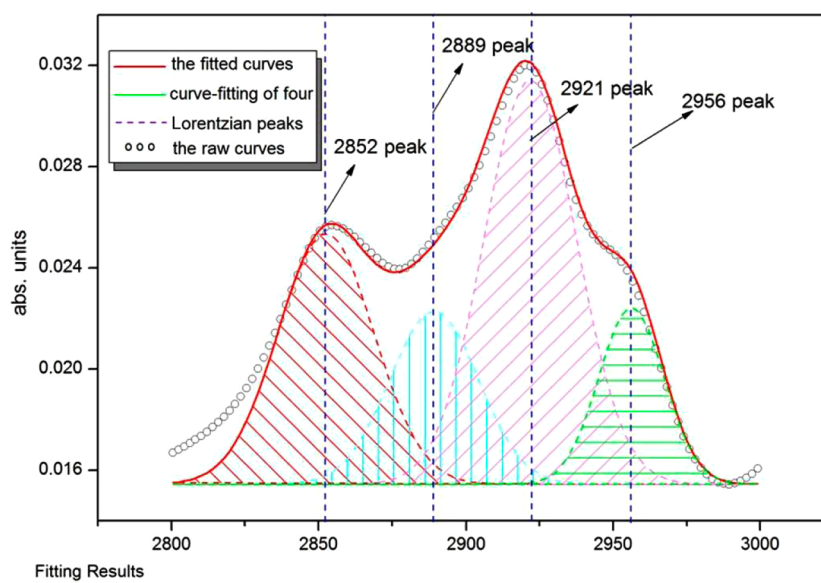
**Figure 6.** FTIR spectra of 2800–3100 cm^{-1} of LJTV, LJTV-350, and LJTV-550.

bending, increases in intensity in all vitrinite. The peak centered at approximately 1329 cm^{-1} mainly corresponds to ether or ester

functional groups. An absorption band at 900–750 cm^{-1} representing aromatic C–H out-of-plane deformation is observed in the FTIR spectra of all vitrinite.

We have magnified the spectra in the region of 3100–2800 cm^{-1} to compare the peak positions (Figure 6). There are three peaks (2957, 2923, 2853 cm^{-1}) in the 2800–3100 cm^{-1} region for sample LJTV. The 2957, 2923, and 2853 cm^{-1} peaks correspond to asymmetric –CH₃ vibration, asymmetric –CH₂– vibration, and symmetrical –CH₂– vibration, respectively. The intensity of these peaks is high before pyrolysis and then decreases after 350 °C. The 2957 cm^{-1} position, a shoulder peak, decreased after 550 °C. The intensity of the 3042 cm^{-1} peak is greater than that of the 3023 cm^{-1} peak. The rate of intensity reduction is greater for the peak at 3042 cm^{-1} than for that at 3023 cm^{-1} . Both of these peaks are almost nonexistent at high temperatures, with only the 3009 cm^{-1} peak remaining. The wavenumbers of the asymmetric –CH₃ and –CH₂– vibrations shift to higher values as the temperature increases.

Table 3 presents the changes in some of the main functional groups with increasing temperature. The functional groups (aromatic C=C ring, aliphatic C–H stretching, aromatic C–H



Peak #	Peak Type	Area Fit T	FWHM	Max Height	Center Grvty	Area Fit TP
1	Gaussian	0.40421	38.34862	0.00991	2852.49522	27.12921
2	Gaussian	0.25855	35.45565	0.00685	2889.20999	17.3529
3	Gaussian	0.63197	37.13761	0.01599	2921.81166	42.41582
4	Gaussian	0.19521	26.3058	0.00697	2956.21091	13.10207

Figure 7. Expanded aliphatic C–H stretching regions (3000–2800 cm^{-1}) and the curve-fitted spectra acquired from sample LJTV-350.

Table 3. FTIR Absorption Band Intensity of Samples of Different Maturities^b

sample no.	Ro,max (%)	aliphatic C—H stretching (3000–2800 cm ⁻¹)	carbonyl/carboxyl C=O stretching (1800–1650 cm ⁻¹)	aromatic C=C ring stretching (1650–1520 cm ⁻¹)	aliphatic —CH ₂ — and —CH ₃ deformation (1520–1350 cm ⁻¹)	aromatic C—H out-of-plane deformation (900–750 cm ⁻¹)
LJTV	1.61	VS	W	VS	VS	VS
LJTV-350 ^a	1.43	VS	W	VS	VS	VS
LJTV-360	1.50	VS	W	VS	VS	VS
LJTV-370	1.49	VS	W	VS	VS	VS
LJTV-380	1.42	VS	W	VS	VS	VS
LJTV-390	1.68	VS	W	VS	VS	VS
LJTV-400	1.67	VS	W	VS	VS	VS
LJTV-410	1.85	S	VW	VS	VS	S
LJTV-420	2.08	S	VW	VS	VS	VS
LJTV-430	2.22	S	VW	VS	VS	S
LJTV-440	2.33	S	W	VS	S	VS
LJTV-450	2.30	S	W	VS	S	VS
LJTV-460	2.36	S	W	VS	S	S
LJTV-470	1.56	S	W	S	W	S
LJTV-480	2.47	W	VW	S	W	S
LJTV-490	2.46	W	VW	S	W	S
LJTV-500	2.64	W	VW	S	VW	S
LJTV-510	2.58	W	VW	S	W	S
LJTV-520	2.80	W	VW	S	W	S
LJTV-530	2.11	W	VW	S	VW	W
LJTV-540		W	VW	S	VW	W
LJTV-550	3.37	VW	VW	S	A	VW

^aLJTV-350 means the vitrinite separated from Lijiatuo mine sample at 350 °C by heating at 10 °C/h. ^bVS = very strong (max height > 0.01 units), S = strong (max height: 0.005–0.01 units), W = weak (max height: 0.0025–0.005 units), VW = very weak (max height: 0.0025–0.005 units), A = absent (max height < 0.001 units).

Table 4. FTIR Indexes Deduced from FTIR Spectra during Pyrolysis

sample no.	CH _{al} 3000–2800 cm ⁻¹	CH ₂ /CH ₃	Al/OX	Al/C=C	C=O/C=C	C=O cont	C=C cont	A factor	C factor
LJTV	0.99	2.96	0.52	0.64	0.22	0.18	0.82	0.39	0.18
LJTV-350	1.41	1.92	0.29	0.31	0.09	0.08	0.92	0.24	0.08
LJTV-360	1.82	1.82	0.51	0.65	0.28	0.22	0.78	0.39	0.22
LJTV-370	1.68	1.59	0.41	0.50	0.22	0.18	0.82	0.33	0.18
LJTV-380	2.74	1.72	0.50	0.62	0.25	0.20	0.80	0.38	0.20
LJTV-390	1.55	1.53	0.32	0.37	0.17	0.15	0.85	0.27	0.15
LJTV-400	1.12	1.58	0.49	0.70	0.43	0.30	0.70	0.41	0.30
LJTV-410	0.59	1.02	0.21	0.25	0.20	0.17	0.83	0.20	0.17
LJTV-420	0.53	1.56	0.25	0.31	0.25	0.20	0.80	0.24	0.20
LJTV-430	0.95	2.34	0.22	0.26	0.16	0.14	0.86	0.21	0.14
LJTV-440	0.52	2.09	0.18	0.20	0.13	0.12	0.88	0.17	0.12
LJTV-450	0.62	2.93	0.20	0.25	0.21	0.17	0.83	0.20	0.17
LJTV-460	0.61	3.77	0.15	0.17	0.13	0.11	0.89	0.14	0.11
LJTV-470	0.83	2.76	0.55	0.63	0.16	0.14	0.86	0.39	0.14
LJTV-480	0.52	3.54	0.41	0.48	0.17	0.15	0.85	0.33	0.15
LJTV-490	0.32	3.31	0.23	0.30	0.33	0.25	0.75	0.23	0.25
LJTV-500	0.21	2.88	0.21	0.27	0.29	0.23	0.77	0.21	0.23
LJTV-510	0.29	3.18	0.32	0.40	0.24	0.19	0.81	0.29	0.19
LJTV-520	0.17	4.32	0.18	0.21	0.16	0.14	0.86	0.17	0.14
LJTV-530	0.34	3.56	0.35	0.43	0.22	0.18	0.82	0.30	0.18
LJTV-540	0.08	4.6	0.13	0.15	0.16	0.14	0.86	0.13	0.14

out-of-plane deformation, aliphatic —CH₂—/—CH₃ deformation) are much more prominent at temperatures below 490 °C. Furthermore, the aromatic C—H stretching out-of-plane deformation, aliphatic C—H bands, aliphatic —CH₂— and —CH₃ deformation, and carbonyl and carboxyl C=O bands decrease in intensity with increasing vitrinite rank of the samples. The stretching intensity of the aromatic C=C ring is high at all temperatures. During pyrolysis, the structural evolution can be divided into three stages

by aliphatic C—H stretching. The intensity of aliphatic C—H stretching is very strong in the first stage (350–400 °C) with band max height of more than 0.01 units, strong in the second stage (400–470 °C) with band max height between 0.005 and 0.01 units, and weak in the last stage (470–550 °C) with band max height between 0.0025 and 0.005.

Structural Parameters of FTIR Analysis. The aliphatic C—H stretching vibrational bands of the FTIR spectra can be used to

Table 5. Semiquantitative Compositions Obtained from ^{13}C CP/TOSS NMR Spectra^a

sample no.	190–165 ppm COO	165–150 ppm aromatic C–O	150–90 ppm aromatic C–C and C–H	90–60 ppm alkyl C–O	60–0 ppm nonpolar alkyl
LJTV	0	0.02	0.67	0.03	0.28
LJTV-350	0.02	0.04	0.77	0.02	0.14
LJTV-360	0.06	0.01	0.76	0	0.17
LJTV-370	0.02	0.03	0.81	0.02	0.12
LJTV-380	0.01	0.05	0.62	0.08	0.24
LJTV-390	0.04	0.02	0.83	0.01	0.1
LJTV-400	0	0.04	0.78	0.01	0.17
LJTV-410	0.05	0.01	0.82	0	0.12
LJTV-420	0.02	0.03	0.83	0.01	0.11
LJTV-440	0.01	0.05	0.87	0.01	0.06
LJTV-450	0.01	0.03	0.9	0.01	0.05
LJTV-460	0	0.03	0.91	0	0.06
LJTV-470	0	0.04	0.91	0.01	0.04
LJTV-480	0.06	0.02	0.84	0.05	0.04
LJTV-490	0	0.03	0.92	0	0.04
LJTV-500	0.06	0.02	0.89	0.02	0.01
LJTV-540	0.02	0.02	0.88	0.01	0.07

^aThe chemical percentages in each row add up to 100%.

Table 6. ^{13}C NMR Structure Parameters of LJTV under Heat Treatment^a

sample no.	$f_{\text{a-c}}$	$f_{\text{a-p}}$	$f_{\text{a-S}}$	$f_{\text{a-B}}$	$f_{\text{a-H}}$	$f_{\text{al-O}}$	$f_{\text{al-H}}$	$f_{\text{al*}}$	$f_{\text{a-N}}$	f_{a}
LJTV	0	0.02	0.08	0.14	0.45	0.03	0.2	0.08	0.24	0.69
LJTV-350	0.02	0.04	0.14	0.2	0.43	0.02	0.07	0.07	0.38	0.83
LJTV-360	0.06	0.01	0.1	0.18	0.48	0	0.09	0.08	0.29	0.82
LJTV-370	0.02	0.03	0.17	0.24	0.4	0.02	0.05	0.07	0.44	0.86
LJTV-380	0.01	0.05	0.15	0.17	0.3	0.08	0.14	0.1	0.37	0.68
LJTV-390	0.04	0.02	0.15	0.23	0.45	0.01	0.04	0.06	0.4	0.89
LJTV-400	0	0.04	0.14	0.21	0.43	0.01	0.1	0.07	0.38	0.82
LJTV-410	0.05	0.01	0.11	0.21	0.5	0	0.04	0.08	0.32	0.88
LJTV-420	0.02	0.03	0.13	0.22	0.48	0.01	0.07	0.04	0.38	0.88
LJTV-440	0.01	0.05	0.15	0.24	0.48	0.01	0.03	0.03	0.45	0.93
LJTV-450	0.01	0.03	0.12	0.23	0.55	0.01	0.02	0.03	0.37	0.93
LJTV-460	0	0.03	0.14	0.26	0.51	0	0.03	0.03	0.43	0.94
LJTV-470	0	0.04	0.15	0.24	0.52	0.01	0.01	0.03	0.43	0.95
LJTV-480	0.06	0.02	0.12	0.23	0.49	0.05	0.03	0.01	0.37	0.91
LJTV-490	0	0.03	0.14	0.25	0.53	0	0.02	0.02	0.42	0.96
LJTV-500	0.06	0.02	0.12	0.25	0.52	0.02	0.01	0	0.39	0.97
LJTV-540	0.02	0.02	0.11	0.24	0.53	0.01	0.04	0.03	0.37	0.92

^a $f_{\text{a-c}}$: carbonyl group or carboxyl group C ($\delta > 165$); $f_{\text{a-p}}$: aromatic C bonded to hydroxyl or ether oxygen ($\delta = 150$ –165); $f_{\text{a-S}}$: alkylated aromatic C ($\delta = 135$ –150); $f_{\text{a-B}}$: aromatic bridgehead C ($\delta = 130$ –135); $f_{\text{a-H}}$: protonated and aromatic C ($\delta = 90$ –130); $f_{\text{al-O}}$: aliphatic C bonded to oxygen ($\delta = 60$ –90); $f_{\text{al-H}}$: CH or CH_2 ($\delta = 25$ –60); $f_{\text{al*}}$: CH_3 or quaternary C ($\delta = 0$ –25); $f_{\text{a-N}}$: nonprotonated and aromatic C; f_{a} : total sp_2 -hybridized C.

evaluate the degree of branching and chain length of the aliphatic side functional groups within the vitrinite macromolecular structure. The spectral region at 3000–2800 cm^{-1} (Figure 7), representing aliphatic C–H stretching, was curve-fitted to derive A2920 cm^{-1} and A2950 cm^{-1} for calculating the CH_2/CH_3 ratio. The spectral region at 1800–1000 cm^{-1} , representing C=O and C=C bending, was then curve-fitted to derive A1800–1650 cm^{-1} , A1650–1520 cm^{-1} , A3000–2800 cm^{-1} , and A1800–1520 cm^{-1} to calculate the A factor, C factor, Al/C=C, Al/OX, A_{ar}/A_{al}, C=O/C=C, C=O cont, and C=C cont. The values of these structural parameters are listed in Table 4.

The ratio CH_2/CH_3 decreases in the early stage of pyrolysis and then increases in the high-temperature stage. The value of this ratio for sample LJTV, 2.96 in Table 4, implies that the side chains attached to the macromolecular structure are 75% $-\text{CH}_2-$ functional groups and 25% $-\text{CH}_3$ functional groups. Table 4 reveals that both the contribution of aliphatic C–H stretching

(area of 3000–2800 cm^{-1}) and the aliphatic/oxygen-containing compounds ratio (area of 3000–2800 cm^{-1} versus OX at 1800–1520 cm^{-1}) decrease. The carbonyl contribution (C=O cont) is lower, whereas the aromatic carbon contribution is high at all temperatures. The ratio of $\text{CH}_{\text{al}}/(\text{CH}_{\text{al}} + \text{C}=\text{C})$ (i.e., the A factor),³² which reflects the hydrocarbon-generating potential, decreases in higher-rank coal.

Carbon Types. ^{13}C NMR is an effective technique for obtaining the carbon type of the vitrinite molecular structure. Shifts of 0–90 ppm are assigned to aliphatic carbon, and shifts of 90–160 ppm are assigned to aromatic carbon. The ^{13}C NMR results for vitrinite samples of different maturities show that the aromatic carbon peak intensity is greater than the aliphatic carbon peak intensity (Table 5, Figure 8). The two main peaks are relatively narrow and concentrated, representing a small distribution of carbon types. With increasing maturity, the relative strength of the aliphatic carbon contribution

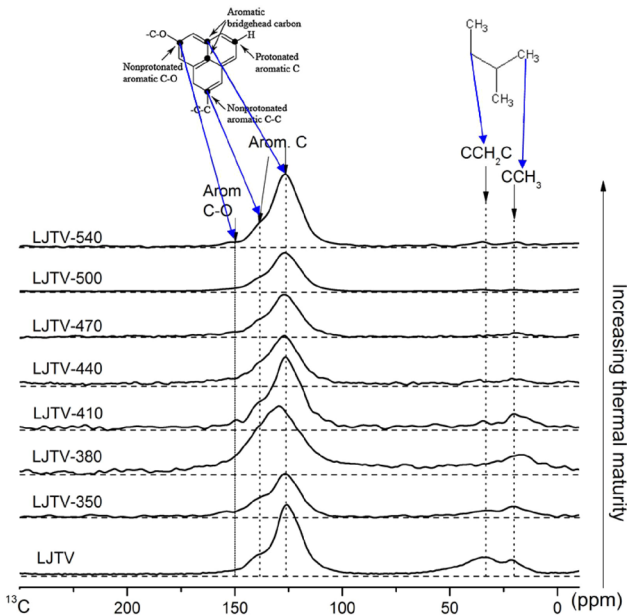


Figure 8. ^{13}C NMR spectra of LJTV vitrinite pyrolysis sediments.

gradually decreases. The carbon structure can be analyzed based on the structural parameters obtained during the pyrolysis process.

Among the aromatic functional groups are bridgehead carbons between several rings. The types of aromatic carbons, which severely overlap between 90 and 165 ppm in the ^{13}C NMR spectra of vitrinite, include bridgehead aromatics, aromatic C–O, protonated aromatic C–H, and nonprotonated aromatic C–C. The overlapped carbons between 0 and 90 ppm are aliphatic carbons. The content of $\text{C}(\text{CH}_2)\text{C}$ functional groups is greater than that of CCH_3 functional groups in the sample LJTV. The CCH_3 groups are eliminated more slowly than the $\text{C}(\text{CH}_2)\text{C}$ groups. From the ^{13}C NMR pyrolysis series, we can see that the occurrence of aliphatic carbon decreases, whereas that of aromatic carbon increases during the pyrolysis process. The aliphatic carbon content is small after 440 °C. The

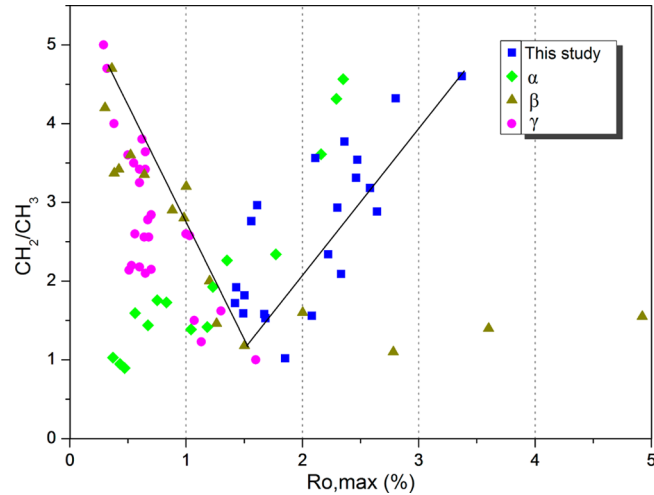


Figure 10. Relational graph of $\text{A}2920\text{ cm}^{-1}/\text{A}2950\text{ cm}^{-1}$ and Ro,max . α : Xin et al.;²⁷ β : Chen et al.;³⁴ γ : Yao et al.³

32 ppm signal is assigned to methyl and methylene, whose rate of decrease is greater than that of methyl (20 ppm) due to their lower stability.

Most of the carbon content in vitrinite pyrolysis was protonated aromatic carbon ($f_{\text{a-H}}$), followed by aliphatic methylene and methane ($f_{\text{al-H}}$), aromatic bridgehead and inner carbon ($f_{\text{a-B}}$), aromatic carbon with alkyl attachment ($f_{\text{a-S}}$), and aliphatic methyl ($f_{\text{al-s}}$).³³ The content of aromatic carbon with oxygen attachment ($f_{\text{a-p}}$) and aliphatic connected carbon and oxygen ($f_{\text{al-O}}$) is 2% and 3%. The content of carboxyl carbon ($f_{\text{a-c}}$) is small (Figure 9). Aliphatic carbon of sample LJTV, with a content of 31% of total carbon, is mainly methyl, methene, and methyne. In the pyrolysis hydrocarbon generation process, the aromatic carbon content gradually increased from a relative content of 0.69 before pyrolysis to 0.83 (an increase of 0.14) after pyrolysis at 350 °C and 0.96 above 490 °C (Table 6).

4.3. Evolution of Structural Parameters during Pyrolysis.

The aliphatic chain length was characterized by $\text{A}2920\text{ cm}^{-1}/\text{A}2950\text{ cm}^{-1}$, which was calculated using the peak

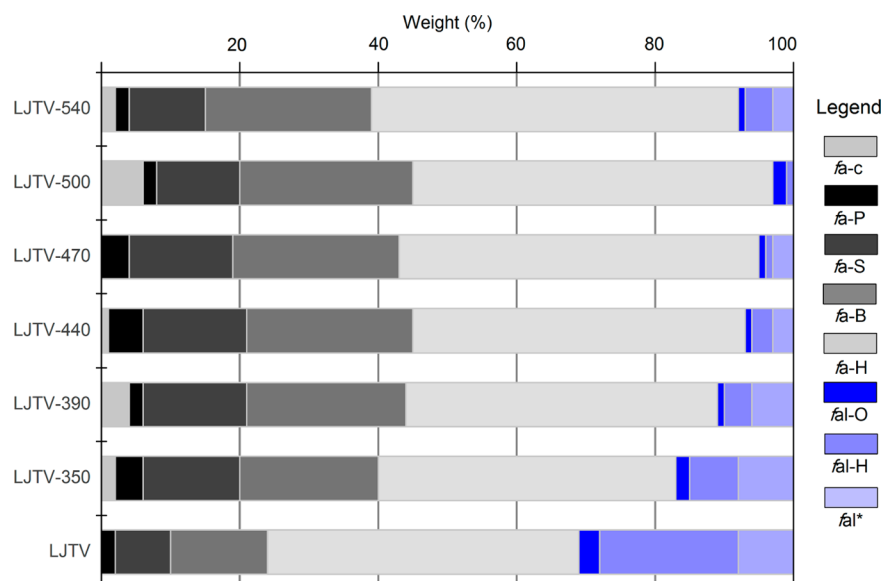


Figure 9. Contents of different types of aromatic and aliphatic carbons in LJTV under heat treatment.

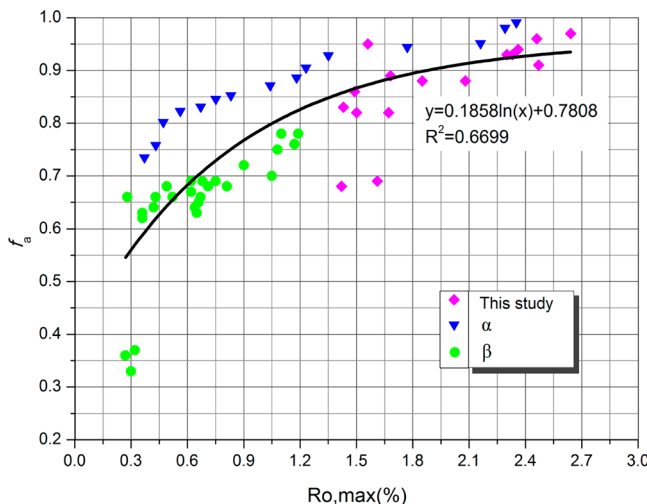


Figure 11. Relational graph of f_a and Ro_{max} . α : Suggate et al.⁶ β : Xin et al.²⁷

areas of the asymmetric stretching vibrations. Chen et al.³⁴ have found that the CH_2/CH_3 ratio steadily decreased from peat to medium-volatile bituminous coal, followed by a highly scattered tail up to anthracite (Figure 10). The weakness of the aliphatic C–H stretching at approximately 2800–3000 cm^{-1} in anthracite and semianthracite might have caused some uncertainties in the calculated CH_2/CH_3 ratios for high-rank coals. Consequently, the trends of both the aromaticity and the chain length ratios were more consistent for low-rank coals, especially for $Ro < 1.50\%$. According to Xin et al.²⁷ and this study, the CH_2/CH_3 ratio increases with maturity when $Ro > 1.60\%$. Thus, we can divide the coalification progress into two stages at $Ro_{max} 1.5\%$ using the value of the ratio CH_2/CH_3 , which first decreases and then increases. On the basis of the structural parameter f_a in particular, the aromaticity of vitrinite increases during pyrolysis (Figure 11). Generally, the carbon types, the accumulation of aromatic carbons, and the content alterations of vitrinite caused by heating during pyrolysis occur due to the removal of aromatic C–O functional groups and the depletion of aliphatic carbons, which is in agreement with the results of earlier studies.

5. CONCLUSIONS

This paper investigates the systematic analysis of the structural and compositional change of coal vitrinite during pyrolysis. In the course of this analysis, we calculated the structural parameters of the vitrinite sample LJTV ($d_{00} = 3.56 \text{ \AA}$, $L_c = 11.62 \text{ \AA}$, $L_a = 10.99 \text{ \AA}$). The FTIR spectra exhibit aliphatic C–H stretching, and the aliphatic/oxygen-containing compounds ratio decreases with increasing rank of vitrinite samples. Additionally, the C=O stretching contribution decreases. In contrast, the value of the aromatic carbon contribution is high for all samples. The A factor, which reflects the hydrocarbon-generating potential, decreases in higher-rank coal ($Ro > 1.61\%$). Additionally, some insights into the chemical structural changes in vitrinite were obtained. The intensity of the aromatic carbon peak is much greater than that of the aliphatic carbon peak. The study of systematic ^{13}C NMR spectra concludes that the content of aliphatic carbon decreases progressively with increasing thermal maturity for the replacement of aromatic hydrogens by condensation. The CCH_3 groups are eliminated more slowly than the $\text{C}(\text{CH}_2)\text{C}$

groups. The CH_2/CH_3 ratio decreases initially and subsequently increases during coalification. On the basis of the structural parameter f_a in particular, the aromaticity of vitrinite increases during pyrolysis.

■ AUTHOR INFORMATION

Corresponding Author

*E-mail: liwucumt@126.com.

Notes

The authors declare no competing financial interest.

■ ACKNOWLEDGMENTS

W.L. would like to thank the China Scholarship Council for financial support. The authors also gratefully acknowledge the support of the National Natural Science Foundation of China (41072117), the Research and Innovation Project for College Graduates of Jiangsu Province (No. CXZZ12_0945), and the Fundamental Research Funds for the Central Universities (No. 2012LWB77).

■ REFERENCES

- (1) Kelemen, S. R.; Afeworki, M.; Gorbaty, M. L.; Sansone, M.; Kwiatak, P. J.; Walters, C. C.; Freund, H.; Siskin, M.; Bence, A. E.; Curry, D. J.; Solum, M.; Pugmire, R. J.; Vandenbroucke, M.; Leblond, M.; Behar, F. Direct characterization of kerogen by X-ray and solid-state ^{13}C nuclear magnetic resonance methods. *Energy Fuels* **2007**, *21*, 1548–1561.
- (2) Wei, Z.; Gao, X.; Zhang, D.; Da, J. Assessment of thermal evolution of kerogen geopolymers with their structural parameters measured by solid-state ^{13}C NMR spectroscopy. *Energy Fuels* **2004**, *19*, 240–250.
- (3) Yao, S. P.; Zhang, K.; Jiao, K.; Hu, W. X. Evolution of coal structures: FTIR analyses of experimental simulations and naturally matured coals in the Ordos Basin, China. *Energy Explor. Exploit.* **2011**, *29*, 1–19.
- (4) Brown, J. K.; Hirsch, P. B. Recent infra-red and X-ray studies of coal. *Nature* **1955**, *175*, 229–233.
- (5) Kuz'mina, L. G.; Churakov, A. V.; Howard, J. A. K.; Vedernikov, A. I.; Lobova, N. A.; Botmanova, A. A.; Alfimov, M. V.; Gromov, S. P. Structural investigation of model compounds for an acceptor component of a new type of charge-transfer complexes based on viologen analogues. Characteristic features of the molecular and supramolecular structures. *Crystallogr. Rep.* **2005**, *50*, 234–253.
- (6) Suggate, R. P.; Dickinson, W. W. Carbon NMR of coals: The effects of coal type and rank. *Int. J. Coal Geol.* **2004**, *57*, 1–22.
- (7) Conte, P.; Spaccini, R.; Piccolo, A. State of the art of CPMAS ^{13}C -NMR spectroscopy applied to natural organic matter. *Prog. Nucl. Magn. Reson. Spectrosc.* **2004**, *44*, 215–223.
- (8) Takanohashi, T.; Kawashima, H. Construction of a model structure for Upper Freeport coal using ^{13}C NMR chemical shift calculations. *Energy Fuels* **2002**, *16*, 379–387.
- (9) Cao, X. Y.; Chappell, M. A.; Schimmelmann, A.; Mastalerz, M.; Li, Y.; Hu, W. G.; Mao, J. D. Chemical structure changes in kerogen from bituminous coal in response to dike intrusions as investigated by advanced solid-state C-13 NMR spectroscopy. *Int. J. Coal Geol.* **2013**, *108*, 53–64.
- (10) Cao, X. Y.; Yang, J.; Mao, J. D. Characterization of kerogen using solid-state nuclear magnetic resonance spectroscopy: A review. *Int. J. Coal Geol.* **2013**, *108*, 83–90.
- (11) Černý, J. Structural dependence of CH bond absorptivities and consequences for FT-i.r. analysis of coals. *Fuel* **1996**, *75*, 1301–1306.
- (12) Geng, W.; Nakajima, T.; Takanashi, H.; Ohki, A. Analysis of carboxyl group in coal and coal aromaticity by Fourier transform infrared (FT-IR) spectrometry. *Fuel* **2009**, *88*, 139–144.

- (13) Cho, W.-t.; Kim, S.; Choi, H.-k.; Rhim, Y.-j.; Lim, J.-h.; Lee, S.-h.; Yoo, J. Characterization of chars made of solvent extracted coals. *Korean J. Chem. Eng.* **2012**, *29*, 190–195.
- (14) Dun, W.; Guijian, L.; Ruoyu, S.; Xiang, F. Investigation of Structural Characteristics of Thermally Metamorphosed Coal by FTIR Spectroscopy and X-ray Diffraction. *Energy Fuels* **2013**, *27*, 5823–5830.
- (15) Everson, R. C.; Okolo, G. N.; Neomagus, H. W. J. P.; dos Santos, J. M. X-ray diffraction parameters and reaction rate modeling for gasification and combustion of chars derived from inertinite-rich coals. *Fuel* **2013**, *109*, 148–156.
- (16) Sun, Q.; Li, W.; Chen, H.; Li, B. The variation of structural characteristics of macerals during pyrolysis. *Fuel* **2003**, *82*, 669–676.
- (17) Guo, Y.; Renton, J. J.; Penn, J. H. FTIR microspectroscopy of particular liptinite- (lopinitite-) rich, Late Permian coals from Southern China. *Int. J. Coal Geol.* **1996**, *29*, 187–197.
- (18) Ibarra, J.; Muñoz, E.; Moliner, R. FTIR study of the evolution of coal structure during the coalification process. *Org. Geochem.* **1996**, *24*, 725–735.
- (19) Walker, R.; Mastalerz, M.; Brassell, S.; Elswick, E.; Hower, J. C.; Schimmelmann, A. Chemistry of thermally altered high volatile bituminous coals from southern Indiana. *Int. J. Coal Geol.* **2007**, *71*, 2–14.
- (20) Komorek, J.; Morga, R. Evolution of optical properties of vitrinite, sporinite and semifusinite in response to heating under inert conditions. *Int. J. Coal Geol.* **2007**, *71*, 389–404.
- (21) Komorek, J.; Morga, R. Vitrinite reflectance property change during heating under inert conditions. *Int. J. Coal Geol.* **2003**, *54*, 125–136.
- (22) Walker, R.; Mastalerz, M. Functional group and individual maceral chemistry of high volatile bituminous coals from southern Indiana: Controls on coking. *Int. J. Coal Geol.* **2004**, *58*, 181–191.
- (23) Morga, R. Chemical structure of semifusinite and fusinite of steam and coking coal from the Upper Silesian Coal Basin (Poland) and its changes during heating as inferred from micro-FTIR analysis. *Int. J. Coal Geol.* **2010**, *84*, 1–15.
- (24) Li, W.; Zhu, Y. M.; Chen, S. B.; Zhou, Y. Research on the structural characteristics of vitrinite in different coal ranks. *Fuel* **2013**, *107*, 647–652.
- (25) Li, M.; Zeng, F.; Chang, H.; Xu, B.; Wang, W. Aggregate structure evolution of low-rank coals during pyrolysis by in-situ X-ray diffraction. *Int. J. Coal Geol.* **2013**, *116–117*, 262–269.
- (26) Dutta, S.; Hartkopf-Fröder, C.; Witte, K.; Brocke, R.; Mann, U. Molecular characterization of fossil palynomorphs by transmission micro-FTIR spectroscopy: Implications for hydrocarbon source evaluation. *Int. J. Coal Geol.* **2013**, *115*, 13–23.
- (27) Xin, H.-h.; Wang, D.-m.; Qi, X.-y.; Qi, G.-s.; Dou, G.-l. Structural characteristics of coal functional groups using quantum chemistry for quantification of infrared spectra. *Fuel Process. Technol.* **2014**, *118*, 287–295.
- (28) Wang, S.; Tang, Y.; Schobert, H. H.; Guo, Y. n.; Su, Y. FTIR and ^{13}C NMR investigation of coal component of Late Permian coals from Southern China. *Energy Fuels* **2011**, *25*, 5672–5677.
- (29) Zhou, Q.; Xiao, X.; Pan, L.; Tian, H. The relationship between micro-Raman spectral parameters and reflectance of solid bitumen. *Int. J. Coal Geol.* **2014**, *121*, 19–25.
- (30) Siddiqui, M. N.; Ali, M. F.; Shirokoff, J. Use of X-ray diffraction in assessing the aging pattern of asphalt fractions. *Fuel* **2002**, *81*, 51–58.
- (31) Yoshizawa, N.; Maruyama, K.; Yamashita, T.; Akimoto, A. Dependence of microscopic structure and swelling property of DTF chars upon heat-treatment temperature. *Fuel* **2006**, *85*, 2064–2070.
- (32) D'Angelo, J. A.; Escudero, L. B.; Volkheimer, W.; Zodrow, E. L. Chemometric analysis of functional groups in fossil remains of the Dicroidium flora (Cacheuta, Mendoza, Argentina): Implications for kerogen formation. *Int. J. Coal Geol.* **2011**, *87*, 97–111.
- (33) Morga, R. Changes of semifusinite and fusinite surface roughness during heat treatment determined by atomic force microscopy. *Int. J. Coal Geol.* **2011**, *88*, 218–226.
- (34) Chen, Y.; Mastalerz, M.; Schimmelmann, A. Characterization of chemical functional groups in macerals across different coal ranks via micro-FTIR spectroscopy. *Int. J. Coal Geol.* **2012**, *104*, 22–33.